RESEARCH ARTICLE | JANUARY 10 2025

Implementation of simultaneous ultraviolet/visible and x-ray absorption spectroscopy with microfluidics

Olivia McCubbin Stepanic ; Christopher J. Pollock; Kara A. Zielinski ; William Foschi ; Derek B. Rice; Lois Pollack ; Serena DeBeer

Rev. Sci. Instrum. 96, 015107 (2025)
https://doi.org/10.1063/5.0218572

Review of Scientific Instruments ARTICLE pubs.aip.org/aip/rsi

Implementation of simultaneous ultraviolet/visible and x-ray absorption spectroscopy with microfluidics

Cite as: Rev. Sci. Instrum. 96, 015107 (2025); doi: 10.1063/5.0218572
Submitted: 12 May 2024 • Accepted: 18 December 2024 •
Published Online: 10 January 2025

Olivia McCubbin Stepanic,[1] Christopher J. Pollock,[2] Kara A. Zielinski,[3] William Foschi,[2] Derek B. Rice,[1] Lois Pollack,[3] and Serena DeBeer[1,a)]

AFFILIATIONS

[1] Max Planck Institute for Chemical Energy Conversion, Mülheim an der Ruhr 45470, Germany
[2] Cornell High Energy Synchrotron Source, Wilson Laboratory, Cornell University, Ithaca, New York 14853, USA
[3] School of Applied Engineering and Physics, Cornell University, Ithaca, New York 14853, USA

[a)] **Author to whom correspondence should be addressed:** serena.debeer@cec.mpg.de

ABSTRACT

X-ray spectroscopies are uniquely poised to describe the geometric and electronic structure of metalloenzyme active sites under a wide variety of sample conditions. UV/Vis (ultraviolet/visible) spectroscopy is a similarly well-established technique that can identify and quantify catalytic intermediates. The work described here reports the first simultaneous collection of full *in situ* UV/Vis and high-energy resolution fluorescence detected x-ray absorption spectra. Implementation of a fiber optic UV/Vis spectrometer and parabolic mirror setup inside the dual array valence emission spectrometer allowing for simultaneous measurement of microfluidic flow and mixing samples at the Photon-In Photon-Out X-ray Spectroscopy beamline is described, and initial results on ferricyanide and a dilute iron protein are presented. In conjunction with advanced microfluidic mixing techniques, this will allow for the measurement and quantification of highly reactive catalytic intermediates at reaction-relevant temperatures on the millisecond timescale while avoiding potential complications induced by freeze quenching samples.

INTRODUCTION

From the first applications of extended x-ray absorption fine structure (EXAFS) to determine metal-ligand bond lengths over 50 years ago, x-ray spectroscopies have been an essential tool for uncovering information on inorganic systems in both crystalline and amorphous solid samples.[1,2] Since then, element selectivity and applicability to a wide range of sample environments have enabled x-ray absorption (XAS) and x-ray emission spectroscopies (XES) to be broadly applied within the (bio)catalysis community, where they have been used to discern geometric and electronic structural details of catalytic intermediates.

Historically, x-ray spectroscopic measurements on biological catalysts have been performed on samples at cryogenic temperatures, conditions that are advantageous by mitigating x-ray induced photodamage and enhancing EXAFS signals due to reduced thermal motion and improved Debye–Waller factors.[3,4] Studies on reaction intermediates were made possible by rapid freeze quench (RFQ) methods. Samples prepared in this manner may be probed by a variety of spectroscopic methods—including Mößbauer, resonance Raman, and electron paramagnetic resonance (EPR)—and thus, x-ray spectroscopic data could be correlated with that from other methods under identical conditions.

Unfortunately, frozen samples necessarily deviate from chemically relevant conditions for the vast majority of catalytic systems, and indeed, x-ray crystallography has documented numerous cases where the very act of freezing a sample can alter its structure.[5–9] Modern interest in x-ray methods has thus motivated an expansion of the range of sample conditions that can be routinely measured. The ever-increasing incident flux provided by synchrotron sources has enabled increasingly dilute samples to be probed, capabilities that have fueled interest in examining catalytic systems under *in situ* or *operando* conditions. Particularly for biological samples, these conditions often involve samples in a liquid solution between 4 °C

and room temperature and thus differ substantially from traditional cryogenic samples.[2,10,11] This sample diversification leads to new opportunities—the ability to collect time-resolved data on chemical reactions under (bio)chemically relevant conditions—and also new challenges, such as how to manage elevated sample sensitivity to photodamage and how to characterize increasingly complex, dynamic sample mixtures.[11–18] To date, several successful studies have been conducted with *operando* XAS cells[13,14,19] or more simplistic flow cells, and similar *in situ* experiments have been performed in SAXS (small angle x-ray scattering)[20–22] though x-ray spectroscopic studies on well-characterized reaction mixtures have so far been lacking.

In the context of metalloenzymes, access to *in situ* x-ray-based mixing experiments has recently been improved by advances in microfluidic mixing.[20,21,23] Prior to the introduction of microfluidics, the sheer quantity of the sample required for XAS and XES measurements (often hundreds of ml) rendered them overwhelmingly inaccessible to proteins of interest. Modern microfluidic experiments allow for the rapid mixing of an enzyme with substrate/reactants to probe dynamics on the sub-millisecond to second scale and enable reaction intermediates to be probed under biologically relevant conditions. Such rapid mixing experiments can be compared to stopped-flow and RFQ techniques, but it is vital to recognize that these *in situ* experiments are conducted in a continuous laminar flow design, where sample flows past the x-ray beam and the timepoint is determined by the flow rate and distance from the mixing point rather than aging in front of the beam, which at room temperature would most often irreversibly damage the sample before data could be collected. Conveniently, this continuous flow methodology also permits a variety of reaction times to be accessed by a combination of changing flow conditions and performing measurements at different spatial locations along a flow cell. Additionally, the overall x-ray dose is significantly lower because the time the sample spends in the beam is determined by flow rates, rather than the time required to collect a single x-ray scan. Flow rates can be modified to ensure that beam exposure time for the sample is orders of magnitude lower than would be the case for a traditional x-ray energy scan, often removing the need to attenuate the incident x-ray beam.

The cylindrical symmetry of some microfluidic mixing cells allows for flexible access to various spectroscopic probes, including the incident x-ray beam, and enables both XAS and XES measurements to be performed. Of particular interest for biological samples is the ability to conduct high energy resolution fluorescence detected x-ray absorption spectroscopy (HERFD XAS) experiments, which provide higher spectral resolution and lower background signal as compared to traditional XAS techniques.[24] The improved resolution can permit a refinement of the pre-edge features that is not possible with the transmission or partial fluorescence yield measurements.[25]

One challenge faced in x-ray spectroscopic studies of flowing solutions is that these samples are almost inherently mixtures of closely related chemical species (e.g., reactant, intermediate, and product complexes) which cannot be easily resolved at the relatively low resolutions of hard x-ray spectra (>1 eV). While statistical tools, such as principal component analysis or constrained matrix factorization,[26] can allow for the deconvolution of spectra into individual components, these methods require the collection of multiple timepoints, which may not be experimentally achievable for all systems. A perhaps more convenient and generally applicable approach would be to collect simultaneous data using a different spectroscopic technique, which would allow for individual species present to be identified and quantified. Indeed, simultaneous measurement of non-HERFD x-ray techniques and orthogonal species-quantitative spectroscopies has proven incredibly useful for an array of *operando* and *in situ* experiments.[27–29]

Due to the often strong absorption of light by protein amino acid side chains and metallocofactors in the ultraviolet and visible regions of the spectrum, ultraviolet/visible absorption spectroscopy (UV/Vis) is a promising candidate for such an orthogonal probe and has been widely applied to study (metallo)enzymes and their reactive intermediates. Especially when paired with stopped-flow techniques, UV/Vis has been used to monitor and quantify enzyme species, including transient intermediates, on the milliseconds to seconds timescale.[30] Indeed, stopped-flow UV/Vis has been used extensively in the dissection of metalloenzyme kinetics, where its ability to quantify individual species—even within complex mixtures containing reactant, product, and intermediate(s)—makes it an invaluable tool.[31] This power to selectively quantify individual species makes UV/Vis an attractive complement for *in situ* x-ray spectroscopic methods. Simultaneous UV/Vis measurements have the advantage of directly quantifying the species of interest at the same time as the x-ray data collection for a single timepoint while avoiding complications induced by performing parallel measurements at different samples/conditions.

Herein, we describe an instrument designed for simultaneous optical and x-ray spectroscopic measurement of the same sample volume, which will allow for speciation information to be obtained concurrently with x-ray spectroscopic data and also for subsequent deconvolution of *in situ* x-ray data into individual component spectra. By combining the Dual Array Valence Emission Spectrometer (DAVES)[32] at the Photon-In Photon-Out X-ray Spectroscopy (PIPOXS) beamline at the Cornell High Energy Synchrotron Source (CHESS) with a fiber optic UV/Vis assembly, simultaneous dual-spectroscopic monitoring of a microfluidic mixer was achieved, which will pave the way for future measurements of discrete timepoints. This work is, to the authors' knowledge, the first pairing of laminar flow microfluidic mixers with simultaneous HERFD XAS and UV/Vis, which will enable the study of chemical intermediates.

EXPERIMENTAL

This section describes the hardware needed to perform the simultaneous measurement as well as a brief protocol for data collection using the mixer.

Hardware

A Flame-T-UV-VIS-ES spectrometer (200–850 nm), deuterium tungsten light source (210–25000 nm), and fiber optic cables from Ocean Insight were used. The source fiber optic cable had a 200 μm aperture, while the detector cable had a 500 μm aperture. The optical design of the UV/Vis spectrometer can be considered to be made up of two discrete assemblies, one for the light source and the other for the detector, each mounted to a translating platform. Each of these assemblies contained three components: the

light source/detector fiber optic cable and two mounted mirrors, all of which were mounted onto aluminum posts. Uncoated parabolic mirrors (Thorlabs) with focal lengths of 76.2 mm (Thorlabs code: MPD139-F01) and 101.6 mm (MPD149-F01) were used between the light source and sample and focal lengths of 15.0 mm (MPD00M9-F01) and 25.4 (MPD119-F01) mm between the sample and the detector. Kinematic mounts, posts, manual translation stages, and rails, in addition to other mounting components, were also purchased from Thorlabs. Two sets of larger translation stages for motorization, here referred to as "translating platforms" (Newport), were connected to stepping motors to control translation in the horizontal plane. These platforms were mounted onto vertical translation stages, which were then mounted to the DAVES spectrometer. Additional notes on alignment are detailed in Appendix A.

Data collection

For all flow experiments, a cone opening Kenics mixer[20] with a quartz capillary of wall thickness 20 μm (Hilgenberg Gmbh.) was used (Appendix B). Ferricyanide was purchased from Sigma-Aldrich, and protein for preliminary experiments was provided by Rahul Banerjee and John Lipscomb. Protein solutions were prepared as solutions of 2 mM Fe (0.5 mM protein) in a 100 mM MOPS buffer (pH 7.0). The sample was flowed through one side of the Kenics mixer, with either water (in the case of ferricyanide) or buffer (in the case of protein) flowing through the second side; thus, the mixing reaction is in this case simulated by a dilution reaction. The sheath flow contained water for ferricyanide and buffer for the protein.

The UV/Vis spectrometer was installed on the PIPOXS beamline (ID2A) at CHESS, and data were collected under ring conditions of 125 mA at 6 GeV. The incident beam energy was selected using a cryogenically cooled Si(311) monochromator and calibrated using the first inflection point of an Fe foil (7111.2 eV); incident and transmitted beam intensities were measured using N_2-filled ion chambers. The Fe Kα_1 signal was energy-selected using five spherically bent Ge(440) analyzer crystals (R = 1 m) mounted to the DAVES spectrometer together with a Pilatus 100 K detector; HERFD spectra were collected with the spectrometer set to the maximum intensity of the Kα_1 emission line. The flight path between the sample, analyzers, and detector was filled with helium to minimize attenuation of the Kα signal. The size of the beam at the capillary can be tuned using a pair of Rh-coated focusing mirrors upstream of the sample from 100 (v) × 400 (h) μm to 1.0 (v) × 2.0 (h) mm; in the present case, the size was set to ~400 × 400 μm^2 so as to match the size of the UV/Vis beam at the sample. Energy scans were performed over the range of 7105–7150 eV in the step scanning mode, with 5 s dwell time per 0.25 eV step; because the overall dwell time is no longer linked to sample exposure, the dwell time was decided based on the desire to maximize signal collection time vs motor movement time and the requirement of having multiple overlaying scans to demonstrate sufficient stability of the sample stream. Normalization scans were performed over a range of 7000–7400 eV with 5 s dwell time per 2 eV step. The sample was delivered to the beam using a microfluidic mixer cell, as described by Zielinski *et al.*,[20] at a total flow rate of 27.5 μl/min (6 μl/min for each half of the mixer and 15.5 μl/min for the outer, sheath flow).

General considerations

The goal for implementing a UV/Vis spectrometer in conjunction with microfluidic sample delivery during HERFD x-ray spectroscopic measurements was to enable simultaneous, quantitative collection of both data types. Both HERFD XAS and UV/Vis spectroscopy have their own requirements with regard to the concentration and size (or path length) of the sample. In the present case, the microfluidic mixer was enclosed by a capillary with an inner diameter of 800 μm, which is well-suited for sample stream diameters of 300–500 μm. In order to collect both x-ray and UV/Vis data on the same cell, tubing, which is transparent to both optical light and x rays, is needed. Here, quartz was selected as it is optically transparent (unlike polyimide/Kapton) and more resistant to x-ray damage than organic polymers, such as polycarbonate. It is best practice to match the sample stream width to that of the x-ray and UV/Vis beams.

In terms of accessible concentrations, HERFD XAS measurements are often performed on samples with as low as 1 mM of the absorbing element; experiments at lower concentration are possible though the signal decreases linearly with concentration and contamination from spurious background signals becomes increasingly significant below ~1 mM. Since the data collection time at synchrotrons is limited, it is generally preferable to have the highest concentration possible of the element being studied, with the upper limit often being imposed by the solubility of the protein. As such, the UV/Vis must be able to operate with sample concentrations at the ~1–10 mM level.

The signal in optical absorption spectroscopy is determined by the product of the sample concentration, extinction coefficient (ε), and path length through the absorbing material, so the accessible sample concentrations are intimately linked to the experimental setup and the details of the sample itself. While traditional UV/Vis spectrometers use a square cuvette and, thus, have an easily defined path length (often 10 mm), the cylindrical capillary of the microfluidic mixer has an effective path length that is much smaller (diameter <1 mm) and can be defined as $\pi d/4$ to account for the circular cross section of the capillary. In the present case, the sample stream diameter was 400 μm and the linear range of absorption for the UV/Vis spectrometer was 0.01–1.0, yielding an acceptable range of sample ε for a 1 mM sample of 0.3–30 mM^{-1} cm^{-1}. This range will scale inversely with the sample concentration, so higher concentration samples permit lower ε values. Notably, the absorption coefficients of ligand to metal charge transfer (LMCT) bands are often found within this range, and thus this instrument can effectively monitor samples that possess such spectral features. Absorption at 280 nm from aromatic amino acids in protein samples, on the other hand, will generally be much too strong for accurate quantification.

In order to achieve simultaneous spectroscopic measurement, the UV/Vis and x-ray spectrometers must probe the same volume of the sample:[27] the beams should have near-identical size and be aligned to the same position on the sample cell. While this is conceptually simple, implementation requires consideration of the geometries for both spectroscopies. Both reflectance and transmission UV/Vis spectrometers are widely available; however, the wider distribution of path lengths generated by a reflectance measurement makes quantitative analysis significantly less accurate than transmission measurements.[33] Additionally, as the sample probed here is

not homogeneous due to the sample and sheath "layers," reflectance measurements would preferentially probe the outer sample area, which is lower in concentration. In cases where a diffusive mixer is used rather than a Kenics mixer, this outer sample area also is at the higher end of the timepoint range, which would result in the x-ray and UV/Vis measurements probing a different sample volume. As such, a transmission UV/Vis spectrometer was used for these measurements.

Focusing elements for the UV/Vis result in a circular spot at the sample, while the incident x-ray beam at PIPOXS has a minimum spot size of ~100 × 400 μm^2. In order to achieve near identical size while making the most efficient use of the 400 μm diameter sample stream, both x-ray and UV/Vis beams were focused to a spot of ~400 × 400. Due to the size and beam divergence of commercially available fiber optic cables, additional optical elements were necessary to achieve a 400 μm diameter spot at the sample cell. Additionally, the fragility of the sample cell capillary made it prudent to keep separately moving components relatively far apart (e.g., 2 cm or more) to avoid potential collisions during alignment, even for the UV/vis components outside of the x-ray spectrometer. Available collimators have focal lengths at and above 1.5 mm, resulting in a beam that is at least 660 μm. Thus, for both the source and detector assemblies, both a collimating and a focusing element were used. To avoid the chromatic aberrations and absorption of lower wavelengths that would occur with focusing lenses, a series of four UV-enhancing parabolic mirrors were used to collimate and focus the beam before and after the sample (Fig. 1).

The HERFD XAS spectrometer relies on Rowland geometry,[2] where the sample, a series of spherically bent analyzer crystals, and the detector are placed along a circular path such that the fluorescence from the sample is diffracted off the crystals and focused into the detector. In the current implementation of DAVES, the analyzer crystals are set below the sample/paths of the incident beams. As such, one assembly of the UV/Vis spectrometer (here, the source assembly) must be placed "within" DAVES and be positioned such that it does not interfere with the movement of the x-ray spectrometer or block sample x-ray fluorescence from reaching the analyzer crystals (Appendix C). The allowed proximity of the UV/Vis spectrometer components to the sample is dependent on the position of the analyzer crystals, which is determined by the analyzer crystal reflection and the required Bragg angle for a given x-ray emission energy. For Fe $K\alpha_1$ emission collected using 1 m radius Ge(440) analyzer crystals, the required Bragg angle is 75.4°, resulting in an angle of incidence of ~14.6°, which restricts the UV/Vis instrumentation to dropping no more than 2.6 cm below the horizontal plane containing the x-ray beam at ~10 cm from the sample capillary. Other implementations with different Bragg angles would permit closer/farther positioning of the UV/Vis focusing lenses relative to the sample. Fortunately, the DAVES spectrometer provides additional flexibility due to its ability to "cant" (rotate) the Rowland circle, as is described in Appendix C, which can enable installation of the UV/Vis even for very high Bragg angle XES measurements.

Design of the UV/Vis apparatus

The UV/Vis instrument can be conceptualized as two assemblies—one for the visible light source and the other for the visible light detector—that can move independently of one another and together make up the overall apparatus. The source assembly (Fig. 2, left) contains the fiber optic source cable, a collimating mirror (M1) to collect the visible light, and a focusing mirror (M2) that focuses the light onto the sample capillary. Similarly, the detector assembly (Fig. 2, right) consists of a collimating mirror (M3) that captures the visible light after it has passed through the sample, a focusing mirror (M4) to direct that light to the detector, and finally the detector fiber optic cable. Each of these assemblies sits on a stack of translation stages that allow for independent motorized movement along the x (transverse to the x-ray beam), y (parallel to the x-ray beam), and z (vertical) axes, enabling the UV/vis to be aligned to itself, the sample, and the x-ray beam.

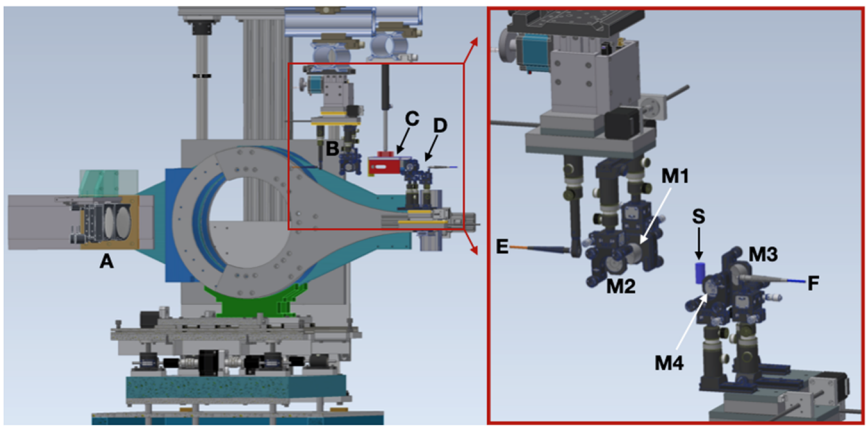

FIG. 1. (Left) A 3D diagram looking upstream of DAVES with the UV/Vis assemblies mounted inside. (a) The array of x-ray analyzer crystals. (b) UV/Vis source assembly. (c) Ion chamber directly prior to the sample. (d) UV/Vis detector assembly. The x-ray detector and sample have been omitted for clarity. (Right) A zoomed-in view of the UV/vis spectrometer with individual components labeled and sample position shown in blue (sample not to size); the source assembly is shown on the left and detector assembly is shown on the right. (e) UV/Vis source fiber optic cable. (f) UV/Vis detector fiber optic cable. Mirrors are numbered in order starting from the UV/Vis source.

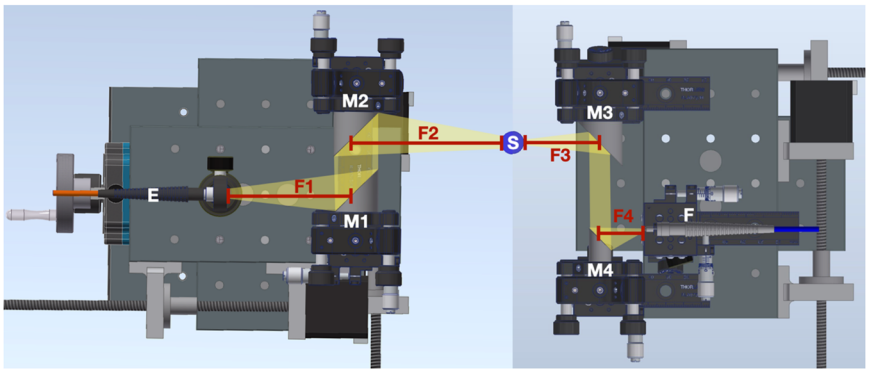

FIG. 2. UV/Vis source side components (left) and detector side (right) mounted on translating platforms, shown relative to the sample (S) position. The sample not shown to size. Mirrors are labeled in order starting from the UV/Vis source. Focal lengths are labeled as follows: F1: UV/Vis source to M1, F2: M2 to sample, F3: sample to M3, and F4: M4 to UV/Vis detector.

The intensity of the UV/Vis beam at the sample (and thus the sensitivity of transmission/absorption measurements) is partially dictated by the proximity of the first collimating mirror (M1) to the UV/Vis source. M1 must be sufficiently close to the optical light source that it captures as much of the divergent light beam as possible; beyond 57.7 mm, the footprint of the optical light is larger than the mirror and, thus, spills over the edges, lessening the intensity able to be delivered to the sample. As such, a low M1 focal length is preferable. However, the beam size at the sample is determined by the ratio of the focal length of M1 to that of focusing mirror M2, and M2 must be far enough away from the sample to avoid shadowing any of the fluorescence signals from reaching the analyzer crystals (*vide infra*). As a general rule, the diameter of the optical beam ($h1$) at the sample is given as the diameter of the beam at the point of emission ($h2$) multiplied by the ratio of focal lengths of the collimating and focusing mirrors,

$$\frac{f1}{f2} = \frac{h1}{h2}. \tag{1}$$

This ratio is, of course, subject to the quality of the mirrors and alignment of components, and some broadening of the beam waist is to be expected. To obtain a ~400 μm diameter optical beam at the sample (given an incident beam diameter of 200 μm and accounting for the error of the mirror alignment) and maintain a source apparatus distance of around 100 mm, focal lengths of 76.2 mm for M1 and 101.6 for M2 mm were used.

As the sample, the surrounding sheath and quartz tube themselves function as cylindrical lenses, the optical beam is modulated

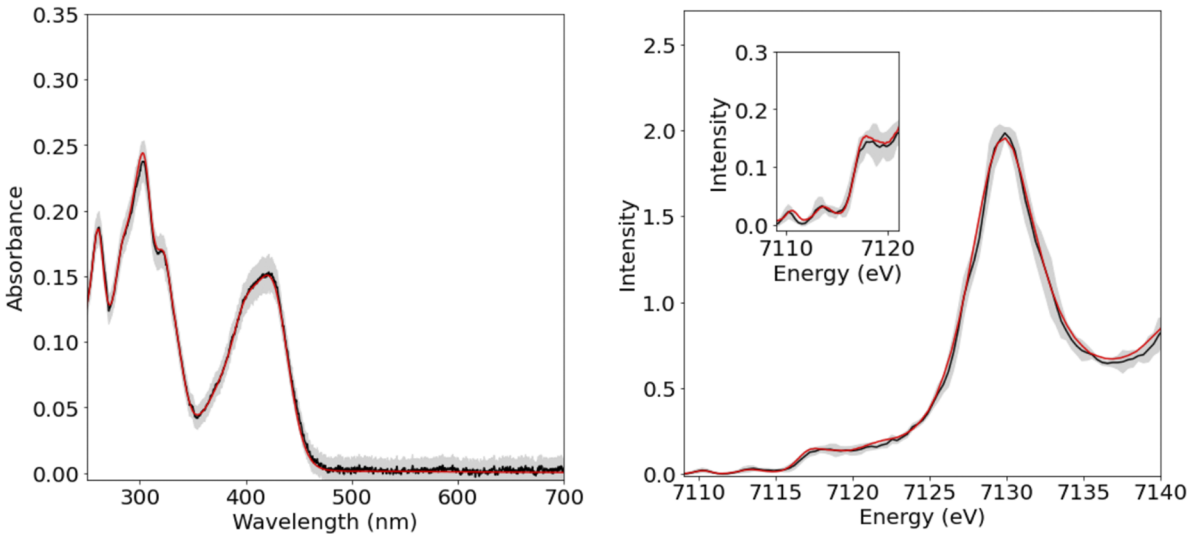

FIG. 3. UV/Vis spectrum (left) of a solution of 5 mM ferricyanide from a standard 1 cm cuvette (red, scaled for best fit) and the microfluidic mixer (black, error shown in gray). K-edge HERFD XAS spectra (right) of 5 mM ferricyanide in aqueous solution (black, error shown in gray) and a solution spectrum of ferricyanide adapted with permission from Huyke *et al.*, J. Synchrotron Radiat. **28**(4), 1100–1113 (2021). Copyright 1999–2024 John Wiley & Sons, Inc. Pre-edges of 5 mM ferricyanide (black, error shown in gray) and the solution spectrum of ferricyanide adapted from Huyke *et al.* (red) are shown as an inset.

in a slightly wavelength dependent fashion by the sample, and rapid optical beam divergence occurs along the horizontal axis. This modulation depends on a series of factors, including the refractive index of the sheath and sample solutions and the relative thickness of each stream. Although it would be beneficial to place the second collimating mirror (M3) very close to the sample, this must be balanced against the danger of having motorized hard objects in close proximity to the fragile sample cell. Here, a focal length of 25.4 mm was used. To decrease the beam size at the detector, a 15 mm focal length mirror was used as the final focusing mirror (M4), resulting in a beam diameter at the detector, which is in any direction 60% (15/25) of the beam after the sample. With perfect alignment in the absence of the sample cell and not accounting for error due to the mirrors themselves, a theoretical spot size of 180 μm could be achieved at the detector. Even so, a detector fiber optic cable with a 200 μm aperture requires exceedingly high precision to align. For experimental ease, a fiber optic cable with a 500 μm aperture was used. This geometry sufficiently accounts for mirror error and the effects of the sample cell and ensures that the entirety of the UV/Vis beam can hit the detector.

Implementation for simultaneous data collection

Initial simultaneous UV/Vis and HERFD data collection was performed on a dilute aqueous solution (5 mM at measurement) of potassium ferricyanide ($K_3[Fe(CN)_6]$), as shown in Fig. 3 (black traces). Ferricyanide has an extinction coefficient of 1.04 mM^{-1} cm^{-1} at 420 nm. With a concentration of 5 mM $K_3[Fe(CN)_6]$ and an effective pathlength of 314 μm, an absorbance of 0.16 is expected; the qualitative shape of the optical spectrum and the quantitative absorbance of A_{420} = 0.152 measured by the fiber optic UV/Vis are thus in excellent agreement with expectation. For comparison, 5 mM ferricyanide UV/Vis data collected utilizing a standard cuvette and previously reported HERFD Fe K-edge XAS data as reported in Ref. 23 are shown in the red traces in Fig. 3. These data confirm that the present setup produces high quality spectra in both the optical and x-ray regime.

The approach for designing an XAS scan for the continuously flowing ferricyanide sample differed notably from how one would approach a static sample. Unlike in traditional XAS measurements, sample damage in experiments on flowing samples is dictated solely by the incident beam flux density and the sample flow rate and is independent of the time spent counting at each energy point. Thus, for given incident beam properties, damage can be assessed by comparing edge scans collected at varying flow rates. In the present case, HERFD edge scans were collected at increasing sample flow rates until the edge profile ceased changing between scans, and this flow rate was assessed as "safe" for collecting undamaged XAS spectra. Furthermore, since the collection time per data point can be arbitrarily long without inducing sample damage, there can be a significant benefit to counting longer at each x-ray energy, rather than collecting multiple short scans, as longer scans reduce the "deadtime" where motors are moving or settling and data are not being collected. UV/Vis scans can easily be collected on the order of a second, and thus the UV/Vis and x-ray data collection may be synchronized such that each x-ray data point is correlated with a corresponding optical spectrum, a feature that is useful to monitor both sample composition and flow stability (*vide infra*).

The data presented in Fig. 3 demonstrate that with collection times of only 5 min on a 5 mM Fe sample, quality HERFD XAS spectra may be obtained on reasonable timescales. Flow stability with ferricyanide, a small and highly soluble molecule, was assessed using Elveflow Coriolis flow sensors and maintained throughout data collection on the order of ±1 μl/min; this was confirmed using the UV/Vis spectra where minimal spectral variations in both the UV/Vis features and baseline position were observed.

This same setup was also used to collect HERFD XAS and UV/Vis data on a soluble iron protein (1 mM Fe at measurement) with an optical absorption feature at 430 nm (ε = 7.5 mM^{-1} cm^{-1}). Other than the lower concentration, the considerations and process for assessing damage and collecting data were identical to those used for ferricyanide. Both UV/Vis and x-ray data were sensitive to variations in flow; in initial experiments, large changes in the UV/Vis baselines over the course of single XANES scans matched variation in XANES scans at the same time (Fig. 4). As such, UV/Vis scans could potentially be used to remove spots with high "flow error" from XANES scans via software correlation of each x-ray data point with a corresponding UV/Vis scan.

Issues with flow stability were occasionally seen mostly due to the increased viscosity of the solution from the protein itself and the added 3% (v/v) glycerol. As shown in Fig. 4, some flow instability is within the error of the experiment and produces little noticeable change in the averaged UV/Vis spectrum or corresponding XAS trace. The red XAS trace and corresponding UV/Vis trace are representative of the data considered "flow stable." The black

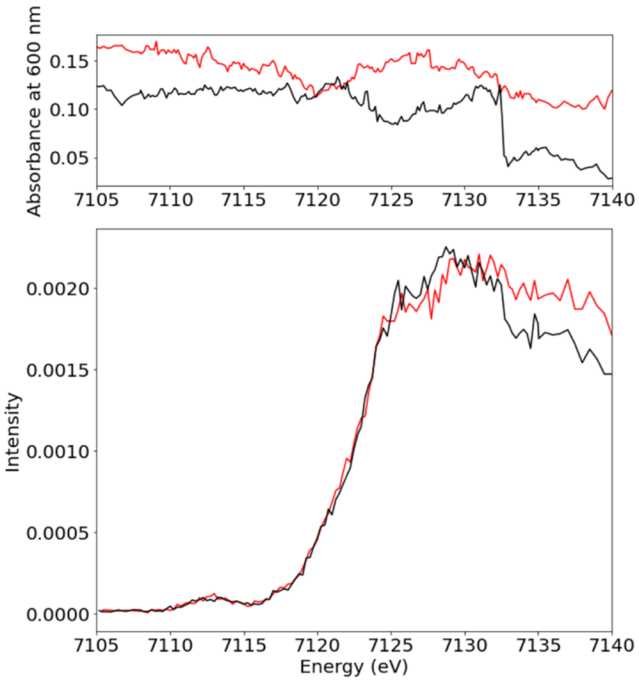

FIG. 4. Representative XAS scans and corresponding UV/Vis absorbance at 600 nm of a 250 μM Fe protein (1 mM Fe). Red traces correspond to sufficiently high stability, while black scans depict large sample flow decrease starting from 7132 eV until the end of the scan.

XANES trace, by contrast, has a significant drop in intensity around 7133 eV. This corresponds to a drop in the baseline absorbance of the UV/Vis scans collected during the same time period. While there is a clear correlation between the two data types, quantification of these changes is difficult as the sample stream may no longer be centered in the capillary, leading to different volumes of samples being probed by XAS and UV/Vis. Additionally, in the case of mixed species, a change in flow rate will result in a different mixing timepoint. Thus, the UV/Vis data may be used to monitor flow stability and "discard" those spectra where there is clear evidence of instability. Such assessments will be important for future kinetic mixing experiments, where flow instabilities could result in erroneous kinetic time points.

CONCLUSIONS/OUTLOOK

In this work, we demonstrate the first simultaneous collection of full *in situ* UV/Vis spectra and HERFD x-ray absorption spectra in combination with flow cells or microfluidic mixers. We have demonstrated that both techniques can be used simultaneously on a capillary for quantitative data collection. In combination with recent advances in microfluidic mixing techniques, this work sets the stage to quantify and describe highly reactive intermediates at temperatures relevant to the reaction itself, without the potentially confounding effects of structural changes that may occur with freezing. A large part of the viability of the two simultaneous spectroscopic techniques used here is that the high concentrations mandated by XAS (which would under typical UV/Vis conditions oversaturate optical spectra) is mediated by the small pathlength, allowing for UV/Vis measurements performed in lab with a 1 cm pathlength cuvette at 31.4 μM to be equivalent to a 1 mM sample with a 400 μm stream diameter. In x-ray techniques requiring lower sample concentration (e.g., SAXS), UV/Vis absorbance measurements are only viable for extremely intense features, such as the 280 nm feature of proteins. In such cases, visible fluorescence may be the preferable paired spectroscopy (direct measurement allows for the accumulation of fluorescence over time, while a low % transmission remains constant and can easily fall into the S/N limit). Additionally, the design shown here can be potentially used with spectroscopies other than UV/Vis. Visible fluorescence has been strongly considered as a future iteration, with the caveat that interactions between the x-ray beam and objects in its path may generate fluorescence in the visible range. This work will hopefully serve as a basis for such additional kinds of simultaneous spectroscopic measurements; this, in combination with the high novelty of combining UV/Vis, one of the most commonly used techniques to identify and quantify intermediates and collect kinetic information on the reaction as a whole, with XAS, a uniquely valuable probe for understanding electronic structure at metallic active sites, sets the groundwork for very exciting experiments to come.

ACKNOWLEDGMENTS

The authors acknowledge the Max Planck Society, the DFG-funded Research Unit "Bioinspired Oxidation Catalysis with Iron Complexes" (Project Nos. 445916766 and DE 1877/4-1 to S.D.), and the National Science Foundation (NSF) (under STC Award No. 1231306 to L.P.) for funding. O.M.S. acknowledges IMPRS-RECHARGE. This work was based on research conducted at the Center for High-Energy X-ray Sciences (CHEXS), which is supported by the National Science Foundation (BIO, ENG, and MPS Directorates) under Award No. DMR-234233. Maurice van Gastel is thanked for helpful discussions. Zachary (Ira) Mathe is thanked for their help in the first beamtime iteration of this assembly.

AUTHOR DECLARATIONS

Conflict of Interest

The authors have no conflicts to disclose.

Author Contributions

O.M.S., C.J.P., and S.D. conceptualized the project. O.M.S. and C.J.P. developed the methodology. K.Z. made the microfluidic mixer cells. Experiments were performed by O.M.S., C.J.P., K.Z., and D.R. O.M.S. performed data analysis. S.D. and L.P. served as project supervisors. O.M.S. wrote the original draft, with sections contributed by K.Z. and C.J.P., and figures constructed by W.H., C.J.P., and O.M.S. All authors reviewed and edited the manuscript.

Olivia McCubbin Stepanic: Conceptualization (equal); Data curation (equal); Methodology (equal); Validation (equal); Writing – original draft (equal); Writing – review & editing (equal). **Christopher J. Pollock**: Conceptualization (equal); Data curation (equal); Methodology (equal); Writing – original draft (equal); Writing – review & editing (equal). **Kara A. Zielinski**: Methodology (equal); Writing – original draft (equal); Writing – review & editing (equal). **William Foschi**: Visualization (equal); Writing – review & editing (equal). **Derek B. Rice**: Data curation (equal); Writing – review & editing (equal). **Lois Pollack**: Supervision (equal); Writing – review & editing (equal). **Serena DeBeer**: Conceptualization (equal); Supervision (equal); Writing – review & editing (equal).

DATA AVAILABILITY

Experimental and simulated data supporting the conclusions of this work are available in the Edmond open data repository of Max Planck Society at https://doi.org/10.17617/3.HJAGE3.

APPENDIX A: ADDITIONAL NOTES FOR IMPLEMENTATION

Thorlabs provides an educational video on aligning parabolic mirrors, which is a valuable resource.[34] There is one absolutely requisite takeaway for aligning the optical beam: the UV/Vis components must be aligned "in order," following the UV/Vis beam path. Alignment of a seven component system can be rather challenging, and it is recommended to mount the optical light source, M1, and M2 on a single platform that is removable from the HERFD x-ray spectrometer; the difficulty of aligning these components rises significantly once they have been mounted inside the spectrometer because of spatial constraints imposed by the spectrometer and the inherent effects of gravity once the platform has been rotated 180° (upside down) to avoid shadowing the analyzer crystals. As

helium filled bags are often placed in the flight path of the x-ray beam, between the sample and the x-ray analyzer crystals, it also may be useful to have a protective cover for this assembly such that the components do not misalign if changes in pressure result in contact between the bags and the optical components. The sample cell is mounted and aligned to the x rays independently, and M3, M4, and the detector can be mounted on a second detachable platform. Aligning the seven-component system outside of the hutch and then treating the aligned "source-M1–M2" and "M3–M4-detector" assemblies as single elements to be aligned to the sample allows for a significantly faster setup experience once access to the hutch is given. In the context of a more permanent setup, or one where severe spatial constraints exist on both sides, mounting M3, M4, and the detector directly into the assembly may be preferred.

The first assembly, containing the UV/Vis source, has the fiber optic cable mounted in a 12.7 mm diameter (1/2 in.) mirror mount using a "SM05SMA" adapter. The mirror mount is then connected to a post, and a post holder is mounted directly to the translating platform. Each mirror is mounted on a kinematic mount and either single direction or xy translation stages (two single translation stages connected together), depending on the necessity of fine movements in a given direction. M1, directly after the UV/Vis source, requires an xy translation stage and has the related post holder mounted directly to the stage. M2 requires only a single translation stage to allow movement along the x axis because the distance between M1 and M2 is arbitrary. For ease of assembly and to avoid jolting or shadowing M1, M2 is mounted onto a rail that extends off of the translating platform.

M3 in theory does not require an additional translation stage as it is part of the "post-sample" translating platform rather than the "pre-sample" translating platform and, thus, can be moved independently of the optical beam and prior mirrors; however, alignment is significantly easier with one. M3 thus has a kinematic mount, a single translation stage along the x axis, post and post holder, and a small dovetail rail. M4 utilizes the same components. The UV/Vis detector fiber optic used had a 0.5 mm aperture and was mounted using a plate holder (FP01), to which it was additionally secured using cyanoacrylate adhesive (Loctite); the authors recommend a ferrule clamp (FCM) for future replications. Here, an xy translation stage is recommended in addition to a rail along the path of the beam for easier realignment.

Once UV/Vis components have been aligned and mounted to the x-ray spectrometer, the sample cell, UV/Vis assemblies, and x-ray beam must be aligned to each other. The coordinate system employed here places the z axis along the vertical, y along the x-ray beam path, and x orthogonal to the path of the x-ray beam (e.g., toward the analyzer crystals). The UV/Vis beam path through the sample thus lies on the x axis. The sample cell was first aligned to the x-ray path in the x direction by scanning the sample x position and monitoring x-ray transmission to find the center of the cell. This step can be performed in the absence of a Fe-containing sample as the relative absorption of the quartz provides enough contrast to determine the center. Then, the tip of the mixer component was found by scanning the z axis in transmission. To avoid burning the mixer component during measurement, the sample was shifted up by 1 mm from the tip such that the x-ray beam sits in the window regime. X-ray to sample alignment in "y" is performed via the x-ray emission (e.g., Kα) scans and, thus, requires a spectroscopic signal from the sample.

Once the sample was aligned to the x-ray beam, the UV/Vis source side was also aligned to the sample. First, the UV/Vis source was moved along the y axis such that the UV/Vis beam was approximately centered on the sample window (for the moment at an arbitrary z). In the event that the UV/Vis source is dramatically off in "x," the focal point will not be near enough to the sample to determine a good center. The focal point was placed at the front of the sample cell and was visualized by placing a piece of paper directly in front of the sample cell. Rough alignment in x and y is thus an iterative process. The UV/Vis source platform was moved rather than the sample since the sample is already aligned to the x-ray beam.

After the UV/Vis source platform has been aligned along both x and y axes, the source platform was moved a defined distance in y such that the focal point remained at the same x-coordinate, but the alignment between the UV/Vis source and UV/Vis detector platforms could be performed without the sample cell in the middle. Alignment was initially performed by moving the UV/Vis detector platform such that the beam sits on the first detector side mirror (M3). Then, the projection off M3 was checked to confirm good collimation, and M4 was realigned such that a good focal point was achieved. Finally, the detector fiber optic cable was aligned by finding the appropriate focal distance and then the maximum intensity was determined by adjusting the rotational x, y, and z positions of the detector and monitoring the intensity using the UV/Vis software. A baseline was collected and absorbance monitoring began. Note that Ocean Optics software has an automatic monitoring, separate from saved spectra, that starts immediately upon launching the UV/Vis absorbance panel within the program; this is not the case for all UV/Vis software.

From this point forward, the UV/Vis source and detector platforms were aligned to each other and should be moved by the same distances in any given direction. The source and detector assemblies together shall thus be referred to as simply the UV/Vis spectrometer. The UV/Vis spectrometer was moved the distance required to return the UV/Vis source to approximately the center of the sample. Next, the UV/Vis spectrometer was moved to scan in y across the sample cell, and the absorbance spectra at each position were used to find the walls of the cell (which scatter and result in a dramatic, wobbly rise in absorbance, or near disappearance of intensity) and the viable collection points in the center of the cell consisting of the cell contents (which show a moderate and linear absorbance due to the solution and quartz of the sample cell, e.g., an absorbance of 0.1 or 0.2, with no scattering effects). By recording the positions of the sample walls and viable collection points, the center in x of the sample window was determined.

Finally, the UV/Vis spectrometer was moved along the z axis to find the tip of the mixer, which increases absorbance and/or causes scattering effects. Since the sample window is often not perfectly straight as changes in z occur so can changes to the true center in x. If the UV/Vis spectrometer must move a considerable distance in z (more than 5 mm), it is highly advisable to recenter in x. Once the tip of the mixer was found along the z-scan of the UV/Vis spectrometer, the UV/Vis spectrometer was moved 1 mm down so that it was aligned to the x-ray beam so that all components were finally and precisely aligned. If realignment is required between the sample x or

y and the x-ray beam, the UV/Vis spectrometer must be moved the same amount. Conversely, *only* the sample should move to change timepoints/sample position in z as the UV/Vis beam and x-ray beam now intersect along the z axis.

In order to collect both x-ray and UV/Vis data on the same cell, tubing, which is transparent to both optical light and x rays, is needed. In the case of UV/Vis, interest in features between 200 and 400 nm precludes the use of polyimide/Kapton (a yellow plastic particularly resistant to damage by x rays). Quartz and polycarbonate are both optically transparent and present potentially viable options. Quartz is the more mechanically rigid and chemically inert of the two; it also allows optical access below 250 nm and is even more resistant to x-ray damage than polyimide. The primary drawback of quartz is a greater attenuation of x rays as compared to polycarbonate or polyimide due to the presence of silicon (as opposed to lighter elements such as carbon, oxygen, and hydrogen); at 7 keV, an empty 800 μm inner diameter quartz cell with 20 μm walls absorbs 27% of the beam, while a 650 μm inner diameter polycarbonate cell with 50 μm walls absorbs just 5%. As such, both options were initially tested; the incident x-ray beam (~7 keV) quickly caused visible discoloration of the polycarbonate tube that precluded concentration calculations based on UV/Vis absorption, and prolonged exposure of the polycarbonate tubing to the x-ray beam eventually led to cell window rupture. No damage to the quartz capillary was observed for the duration of a six-day beamtime, and any issues with sample deposition were removable by cleaning the cell. In the end, despite the relative loss of x-ray signal (the combined result of quartz vs polycarbonate and the wider inner diameter of the tubing for quartz than polycarbonate resulting in additional absorption from the water sheath meant data collected with the quartz cell resulted in experimental data intensity that was ~50% of our polycarbonate option), a quartz cell with a wall thickness of 20 μm was selected as the best available option. In certain cases, although not seen here, quartz has the potential to introduce diffraction spikes into x-ray data if the incident energy spuriously matches a Bragg peak within the quartz crystal; in such cases, borosilicate glass may be preferred.

APPENDIX B: MIXER CHARACTERISTICS AND TIMEPOINT RESOLUTION

A Kenics-style chaotic advection mixer was used for this work.[35–37] In brief, two liquids travel through a sequence of helical mixing elements. After each element, the fluids are stretched, split, and stacked on top of each other to form a series of alternating layers. The number of total layers increases after each element, while the thickness of the layers decreases. Rapid mixing occurs via contacts between the layers as the species quickly diffuse across layers with different compositions. The elements are designed to ensure that the reactants are fully mixed before reaching the end of the Kenics mixer. After exiting the Kenics mixer, the freshly mixed system is surrounded by a co-flowing sheath. This fluid stream continues to flow and age until it intersects the X-ray and UV/Vis beams at a carefully determined position for a desired time delay. For this work, which served to assess the feasibility of signal strength for future mixing experiments, the sample stream was mixed with its underlying solvent (water or buffer, as described in the text). The "mixing reaction" was therefore a dilution "reaction." Flow rates and the position of the beams are easily changed to reach multiple timepoints within the same device.

TABLE I. Effects of flow rate parameters and timepoint determination for both UV/Vis and x-ray spectroscopies.

Sheath flow rate (μl/min)	10.2	15.5
Combined sample flow rate (μl/min)	8	12
Distance from Kenics tip (μm)	4140	6268
Data collection timepoint (ms)	3981	3981
Uncertainty: Parabolic flow profile and Kenics transit time (ms)	340	332
Uncertainty: X-ray beam height (ms)	436	290
X-ray timepoint (ms)	3981 ± 553	3981 ± 441
Uncertainty: UV/Vis beam height (ms)	377	251
UV/Vis timepoint (ms)	3981 ± 508	3981 ± 416

In this work, the cone opening Kenics mixer, as described by Zielinski *et al.*, 2023, was used.[20] This design has eight helical elements housed in a channel with a 100 μm inner diameter. The Kenics mixer was coupled to a quartz capillary with an 800 μm inner diameter, which helps to increase the UV/Vis/x-ray path length of the sample to maximize the signal. The final timepoint captured depends on the sample cell geometry, flow rates of samples A and B (the two species being mixed), the sheath flow rate, and the

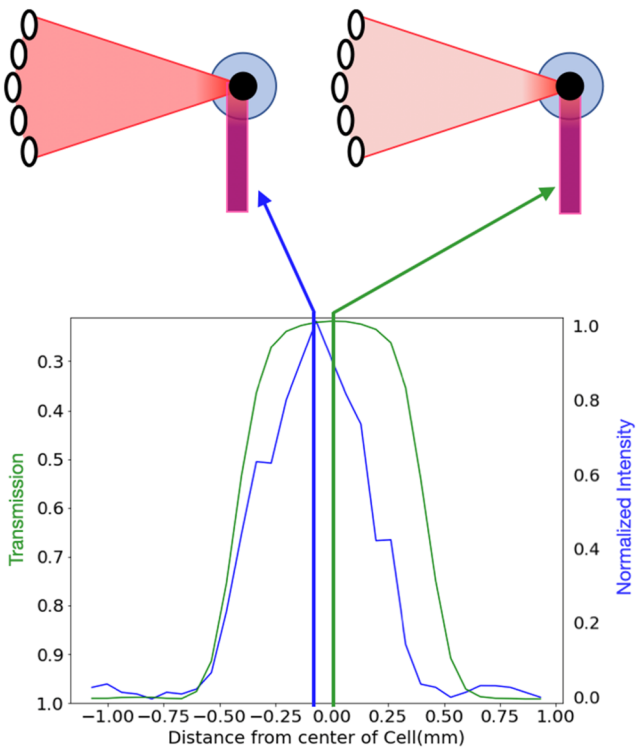

FIG. 5. XAS transmission and fluorescence moving in x across the flow cell, with the position of the sample relative to the beam depicted at both the fluorescence maxima and the cell center.

position of the x-ray and UV/Vis beams relative to the tip of the Kenics mixer. More precisely, the final timepoint is defined by the point of mixing completion inside the Kenics plus the additional travel time through the remainder of the Kenics and the subsequent capillary until it is illuminated by both x-ray and optical beams. The time resolution, which is defined by the uncertainty in the measured timepoint, is influenced by the flow speeds and the size (height) of the x-ray and UV/Vis beams and reflects contributions from the mixing time, delay time, and average travel time through the x-ray and UV/Vis beams. Each component is discussed in more detail below, and the values for two conditions for a set timepoint are shown in Table I.

Complete mixing for the Kenics mixer is defined at a specific position along the blades and is dependent on the size of the components being mixed. For a monoatomic ion, complete mixing occurs after one blade; with a ligand, on the size scale of glucose, after four blades; and with a large molecule, such as a protein, occurs after eight blades. The uncertainty associated with mixing is defined as half the transit time through the Kenics mixer from entry into the mixer to the point of mixing completion and can typically be kept small. After mixing, the flow rates and distance between the fully mixed point to the probe position (the part of the capillary that intersects with x-ray and optical beams) determine the additional delay time. The uncertainty associated with the delay time is due to the parabolic flow profile, or the spread of speeds, across the sample stream in the flow cell.

There is additional uncertainty due to the sample transiting across the finite x-ray and UV/Vis beams based on the travel time through the beam height. This uncertainty is simply calculated as the beam height divided by the average sample velocity in the beam.[25] In this case, both the x-ray and optical beams have a height of 400 μm, so the transit time through the beam should generally be similar. However, in this setup, the UV/Vis beam was centered on the sample cell in the horizontal direction, whereas the x-ray beam was offset 60 μm from the center of the sample cell to maximize counts by slightly reducing the amount of attenuation due to the buffer sheath, as shown in Fig. 5. Thus, the average velocity through the x-ray beam is a little bit slower, and the x-ray timepoint has slightly more uncertainty due to the beam height. This difference should be negligible for longer time points, such as those on the seconds scale. The final uncertainty of the overall timepoint is determined by combining each uncertainty contribution in quadrature. Table I shows

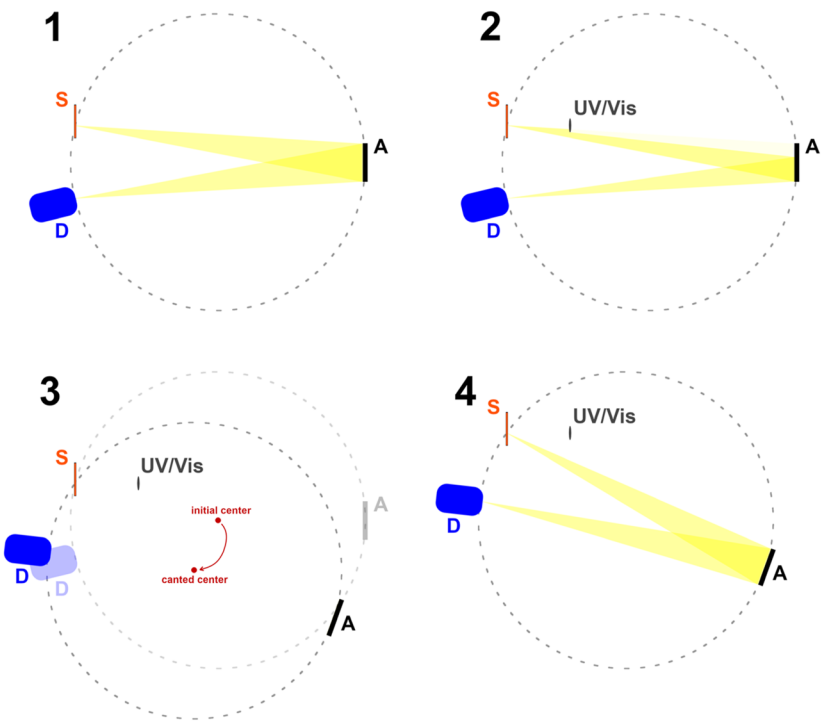

FIG. 6. An illustration of the process of canting the Rowland circle of the DAVES spectrometer; in all panels, the coordinate system is defined as z = up/down and x = left/right, while "S" indicates the sample, "A" indicates the analyzer crystals, and "D" indicates the detector. The beam in these illustrations travels along the y axis (orthogonal to the page) and impinges upon the sample at the point where the sample is intercepted by the Rowland circle. Panel 1 shows the standard operating conditions of DAVES, with the yellow cones depicting the x-ray fluorescence from the sample that is captured by the analyzer array and reflected to the detector. Panel 2 demonstrates how the introduction of the UV/Vis optics can block a portion of the sample fluorescence from reaching the detector, lowering the overall intensity observed from the sample and introducing unacceptable energy-dependent intensity modulations during emission energy scans. Panel 3 depicts how the Rowland circle may be canted by rotation of the circle center about the sample while the UV/Vis components remain in place; both the initial (faded) and canted (full color) positions of the analyzers and detector are shown. Panel 4 finally shows how the new, canted positions allow all of the fluorescence signals to reach the analyzers.

these values, accounting for the average velocity difference between the x-ray and UV/Vis beam.

APPENDIX C: DAVES ROWLAND GEOMETRY CANTING

The requirement that the optical and x-ray beams intercept the sample cell at the same spatial location results in part of the UV/Vis assembly being placed within the DAVES spectrometer. Such an arrangement introduces the possibility for the vertical support structure of the UV/Vis spectrometer to block a portion of the x-ray fluorescence from reaching the analyzer crystals, particularly for analyzers operating at large Bragg angles, i.e., when the vertical offset between the sample and analyzer crystals is small. Fortunately, the DAVES spectrometer is configured in such a way that the Rowland circle(s) may be "canted" by rotation by an arbitrary angle about the sample while leaving all other ancillary equipment in place. An illustration of this process is provided in Fig. 6, demonstrating both how the UV/Vis spectrometer may shadow the analyzer crystals and how a cant of the Rowland circle can remedy this issue.

Mathematically, canting of the Rowland circle may be achieved by transformations of the z (vertical) and x (transverse to the x-ray beam) positions of the Rowland circle center as follows:

$$Z_{new} = -X \sin\theta + Z \cos\theta, \tag{C1}$$

$$X_{new} = X \cos\theta - Z \sin\theta, \tag{C2}$$

where x and z are the original positions of the DAVES spectrometer and θ is the desired canting angle, which may be positive or negative.

It is worth noting that beyond the case presented here where canting may be used to avoid analyzer shadowing by ancillary equipment, Rowland circle canting may also be employed to facilitate two-color operation of DAVES. As noted briefly by Martinie *et al.*,[38] each of the two emission spectrometers of DAVES may be canted independently, providing a strategy to avoid collisions of analyzers/detectors when multiple emission lines are recorded simultaneously.

REFERENCES

[1] D. E. Sayers, F. W. Lytle, and E. A. Stern, "Point scattering theory of X-ray K-absorbtion fine structure," Adv. X-Ray Anal. **13**(13), 248–271 (1969).

[2] G. E. Cutsail III and S. DeBeer, "Challenges and opportunities for applications of advanced X-ray spectroscopy in catalysis research," ACS Catal. **12**, 5864–5886 (2022).

[3] M. M. van Schooneveld and S. DeBeer, "A close look at dose: Toward L-edge XAS spectral uniformity, dose quantification and prediction of metal ion photoreduction," J. Electron Spectrosc. Relat. Phenom. **198**, 31 (2015).

[4] J. Yano, J. Kern, K.-D. Irrgang, M. J. Latimer, U. Bergmann, P. Glatzel, Y. Pushkar, J. Biesiadka, B. Loll, K. Sauer, J. Messinger, A. Zouni, and V. K. Yachandra, "X-ray damage to the Mn_4Ca complex in single crystals of photosystem II: A case study for metalloprotein crystallography," Proc. Natl. Acad. Sci. U. S. A. **102**(34), 12047–12052 (2005).

[5] D. A. Keedy, H. van den Bedem, D. A. Sivak, G. A. Petsko, D. Ringe, M. A. Wilson, and J. S. Fraser, "Crystal cryocooling distorts conformational heterogeneity in a model Michaelis complex of DHFR," Structure **22**(6), 899–910 (2014).

[6] S. Russi, A. González, L. R. Kenner, D. A. Keedy, J. S. Fraser, and H. van den Bedem, "Conformational variation of proteins at room temperature is not dominated by radiation damage," J. Synchrotron Radiat. **24**(1), 73–82 (2017).

[7] T. R. Stachowski, M. Vanarotti, J. Seetharaman, K. Lopez, and M. Fischer, "Water networks repopulate protein–ligand interfaces with temperature," Angew. Chem., Int. Ed. **61**(31), e202112919 (2022).

[8] T. Skaist Mehlman, J. T. Biel, S. M. Azeem, E. R. Nelson, S. Hossain, L. Dunnett, N. G. Paterson, A. Douangamath, R. Talon, D. Axford, H. Orins, F. von Delft, and D. A. Keedy, "Room-temperature crystallography reveals altered binding of small-molecule fragments to PTP1B," eLife **12**, e84632 (2023).

[9] J. S. Fraser, H. van den Bedem, A. J. Samelson, P. T. Lang, J. M. Holton, N. Echols, and T. Alber, "Accessing protein conformational ensembles using room-temperature X-ray crystallography," Proc. Natl. Acad. Sci. U. S. A. **108**(39), 16247–16252 (2011).

[10] J. K. Kowalska, F. A. Lima, C. J. Pollock, J. A. Rees, and S. DeBeer, "A practical guide to high-resolution X-ray spectroscopic measurements and their applications in bioinorganic chemistry," Isr. J. Chem. **56**(9–10), 803–815 (2016).

[11] S. Bordiga, E. Groppo, G. Agostini, J. A. van Bokhoven, and C. Lamberti, "Reactivity of surface species in heterogeneous catalysts probed by in situ X-ray absorption techniques," Chem. Rev. **113**(3), 1736–1850 (2013).

[12] Z. Mathe, D. A. Pantazis, H. B. Lee, R. Gnewkow, B. E. Van Kuiken, T. Agapie, and S. DeBeer, "Calcium valence-to-core X-ray emission spectroscopy: A sensitive probe of oxo protonation in structural models of the oxygen-evolving complex," Inorg. Chem. **58**(23), 16292–16301 (2019).

[13] B. J. Deschner, D. E. Doronkin, T. L. Sheppard, G. Rabsch, J.-D. Grunwaldt, and R. Dittmeyer, "Continuous-flow reactor setup for *operando* x-ray absorption spectroscopy of high pressure heterogeneous liquid–solid catalytic processes," Rev. Sci. Instrum. **92**(12), 124101 (2021).

[14] J. Timoshenko and B. Roldan Cuenya, "*In situ*/*operando* electrocatalyst characterization by X-ray absorption spectroscopy," Chem. Rev. **121**(2), 882–961 (2021).

[15] A. M. Crawford and J. E. Penner-Hahn, "X-ray fluorescence-detected flow cytometry," in *Methods in Molecular Biology*, edited by H. Cellular, N. S. Barteneva and I. A. Vorobjev (Springer, New York, NY, 2018), Vol. 1745, pp. 97–112.

[16] Y. Pertot, C. Schmidt, M. Matthews, A. Chauvet, M. Huppert, V. Svoboda, A. von Conta, A. Tehlar, D. Baykusheva, J.-P. Wolf, and H. J. Wörner, "Time-resolved x-ray absorption spectroscopy with a water window high-harmonic source," Science **355**(6322), 264–267 (2017).

[17] J. Wang, C.-S. Hsu, T.-S. Wu, T.-S. Chan, N.-T. Suen, J.-F. Lee, and H. M. Chen, "In situ X-ray spectroscopies beyond conventional X-ray absorption spectroscopy on deciphering dynamic configuration of electrocatalysts," Nat. Commun. **14**(1), 6576 (2023).

[18] N. Levin, C. Casadevall, G. E. Cutsail, J. Lloret-Fillol, S. DeBeer, and O. Rüdiger, "XAS and EPR in situ observation of Ru(V) Oxo intermediate in a Ru water oxidation complex," ChemElectroChem **9**(3), e202101271 (2022).

[19] P. Jäker, D. Aegerter, T. Kyburz, R. Städler, R. Fonjallaz, B. Detlefs, and D. Koziej, "Flow cell for operando X-ray photon-in-photon-out studies on photo-electrochemical thin film devices," Open Res. Eur. **2**, 74 (2022).

[20] K. A. Zielinski, A. M. Katz, G. D. Calvey, S. A. Pabit, S. K. Milano, C. Aplin, J. San Emeterio, R. A. Cerione, and L. Pollack, "Chaotic advection mixer for capturing transient states of diverse biological macromolecular systems with time-resolved small-angle X-ray scattering," IUCrJ **10**(3), 363–375 (2023).

[21] G. D. Calvey, A. M. Katz, C. B. Schaffer, and L. Pollack, "Mixing injector enables time-resolved crystallography with high hit rate at X-ray free electron lasers," Struct. Dyn. **3**, 054301 (2016).

[22] A. Plumridge, A. M. Katz, G. D. Calvey, R. Elber, S. Kirmizialtin, and L. Pollack, "Revealing the distinct folding phases of an RNA three-helix junction," Nucleic Acids Res. **46**(14), 7354–7365 (2018).

[23] D. A. Huyke, A. Ramachandran, O. Ramirez-Neri, J. A. Guerrero-Cruz, L. B. Gee, A. Braun, D. Sokaras, B. Garcia-Estrada, E. I. Solomon, B. Hedman, M. U. Delgado-Jaime, D. P. DePonte, T. Kroll, and J. G. Santiago, "Millisecond timescale reactions observed via X-ray spectroscopy in a 3D microfabricated fused silica mixer," J. Synchrotron Radiat. **28**(4), 1100–1113 (2021).

[24] G. E. Cutsail, R. Banerjee, A. Zhou, L. Que, Jr., J. D. Lipscomb, and S. DeBeer, "High-resolution extended X-ray absorption fine structure analysis provides evidence for a longer Fe···Fe distance in the Q intermediate of methane monooxygenase," J. Am. Chem. Soc. **14**, 16807 (2018).

[25]K. Hämäläinen, D. P. Siddons, J. B. Hastings, and L. E. Berman, "Elimination of the inner-shell lifetime broadening in x-ray-absorption spectroscopy," Phys. Rev. Lett. **67**(20), 2850–2853 (1991).
[26]P. M. Maffettone, A. C. Daly, and D. Olds, "Constrained non-negative matrix factorization enabling real-time insights of *in situ* and high-throughput experiments," Appl. Phys. Rev. **8**, 041410 (2021).
[27]M. A. Newton and W. van Beek, "Combining synchrotron-based X-ray techniques with vibrational spectroscopies for the *in situ* study of heterogeneous catalysts: A view from a bridge," Chem. Soc. Rev. **39**(12), 4845 (2010).
[28]M. Bauer, G. Heusel, S. Mangold, and H. Bertagnolli, "Spectroscopic set-up for simultaneous UV-Vis/(Q)EXAFS *in situ* and *in operando* studies of homogeneous reactions under laboratory conditions," J. Synchrotron Radiat. **17**(2), 273–279 (2010).
[29]M. Bauer and C. Gastl, "X-ray absorption in homogeneous catalysis research: The iron-catalyzed Michael addition reaction by XAS, RIXS and multi-dimensional spectroscopy," Phys. Chem. Chem. Phys. **12**(21), 5575 (2010).
[30]C. Krebs, L. M. K. Dassama, M. L. Matthews, W. Jiang, J. C. Price, V. Korboukh, N. Li, and J. M. Bollinger, "Novel approaches for the accumulation of oxygenated intermediates to multi-millimolar concentrations," Coord. Chem. Rev. **257**(1), 234–243 (2013).
[31]J. M. Bollinger and C. Krebs, "Stalking intermediates in oxygen activation by iron enzymes: Motivation and method," J. Inorg. Biochem. **100**(4), 586–605 (2006).
[32]K. D. Finkelstein, C. J. Pollock, A. Lyndaker, T. Krawcyk, and J. Conrad, "Dual-array valence emission spectrometer (DAVES): A new approach for hard X-Ray photon-in photon-out spectroscopies," AIP Conf. Proc. **1741**, 030009 (2016).
[33]C. M. Gardner, "Transmission versus reflectance spectroscopy for quantitation," J. Biomed. Opt. **23**(1), 018001 (2018).
[34]Align an Off-Axis Parabolic (OAP) Mirror to Collimate a Beam (Viewer Inspired), Thorlabs Photonics Lab Instructional Video, https://www.thorlabs.de/newgrouppage9.cfm?objectgroup_id=14062#VideoOAPDivtoCol.
[35]S. Wiggins and J. M. Ottino, "Foundations of chaotic mixing," Philos. Trans. R. Soc., A **362**(1818), 937–970 (2004).
[36]E. Saatdjian, A. J. S. Rodrigo, and J. P. B. Mota, "On chaotic advection in a static mixer," Chem. Eng. J. **187**, 289–298 (2012).
[37]A. Bertsch, S. Heimgartner, P. Cousseau, and P. Renaud, "Static micromixers based on large-scale industrial mixer geometry," Lab Chip **1**(1), 56 (2001).
[38]R. J. Martinie, E. J. Blaesi, J. M. Bollinger, C. Krebs, K. D. Finkelstein, and C. J. Pollock, "Two-color valence-to-core X-ray emission spectroscopy tracks cofactor protonation state in a class I ribonucleotide reductase," Angew. Chem., Int. Ed. **57**(39), 12754–12758 (2018).